1 **Two-century sediment records of atmospheric mercury variations in North**

2 **China and their relations with regional and global emissions**

3 Dejun Wan[a,b*], Handong Yang[c], Zhangdong Jin[d], Lei Song[b], Dongliang Ning[a], Longjuan

4 Cheng[a], Qingfeng Jiang[a]

5 [a] School of Geographical Science, Nantong University, Nantong, 226007, China

6 [b] Institute of Hydrogeology and Environmental Geology, Chinese Academy of

7   Geological Sciences, Shijiazhuang 050061, China

8 [c] Environmental Change Research Centre, University College London, London WC1E

9   6BT, UK

10 [d] State Key Laboratory of Loess and Quaternary Geology, Institute of Earth

11   Environment, Chinese Academy of Sciences, Xi'an 710075, China

12

13 **Corresponding authors**:

14 Dejun Wan, dejunwan@foxmail.com, dejunwan@ntu.edu.cn, Address: 999 East

15 Waihuan Road, Nantong, 226007, Jiangsu, China

16 Dongliang Ning, ningdl@ntu.edu.cn, Address: 999 East Waihuan Road, Nantong,

17 226007, Jiangsu, China

18

Abstract

Sedimentary mercury (Hg) records from remote areas are significant for revealing historical variations of regional Hg and understanding the influence of regional and global Hg emissions. In this study, sediment cores were retrieved from two subalpine lakes in Shanxi Province in North China and employed to reconstruct atmospheric Hg variations over the last two centuries. The two records show similar anthropogenic Hg fluxes and evolution trends, corresponding with that they were affected mainly by regional atmospheric Hg deposition. Before ~1950, the records show negligible Hg pollution signals. Atmospheric Hg in the region had increased rapidly since the 1950s, lagged more than a half-century compared to the global Hg. This indicates that they were seldom affected by Hg emissions dominated by Europe and North America after the Industrial Revolution. The Hg increases since the 1950s in the two records corresponded well with rapid industrial developments in and around Shanxi Province after the founding of the PR China, implying the dominant contribution of domestic Hg emissions. By comparing other Hg records, we find that widespread increases in atmospheric Hg in China likely occurred post ~1950. This study rouses to re-examine historical variations in atmospheric Hg at various settings, which is significant to understanding global Hg cycling in the industrial era.

Keyword: sediment record; pollution history; heavy metal; atmospheric pollution; North China

1. Introduction

Mercury (Hg) is one of the most polluted heavy metals on the globe. It is estimated that the global average Hg is about three times higher than that in the pre-industrial era as a result of anthropogenic emissions (Driscoll et al., 2013; Hylander and Meili, 2003). Usually, the largest increases in environmental Hg are found in and around the industrialized regions (Fu et al., 2015; Hylander and Meili, 2003). In the regions, it is estimated that the present atmospheric Hg deposition rate has increased by 2-10 folds (Hylander and Meili, 2003). Historically, in early period of the Industrial Revolution (~1860s-1960s) developed countries in Europe and the United States were the major anthropogenic Hg emitters, accounting for more than 80% of the total global Hg emissions (Streets et al., 2019). Since the 1970s, as developed countries have realized the risks of Hg pollution and put environmental pollution controls in place, Hg emissions in these regions have reduced significantly (Streets et al., 2019). In contrast, in developing countries like China economy and industry have developed rapidly after the Reform and Opening-up in the late 1970s. The development has caused sharp increases in Hg emissions. Now, China contributes the largest amount of anthropogenic Hg into the atmosphere in the world (Fu et al., 2016), accounting for 25-40% of the global total anthropogenic Hg emissions (UNEP, 2018). Therefore, special attentions should be paid to the long-term variations in anthropogenic Hg in China.

In recent decades, some studies reconstructed historical variations of Hg using

61 sedimentary records in different regions of China, such as on the Qinghai-Tibet

62 Plateau (Kang et al., 2016; Yang et al., 2010), in western (Zeng et al., 2014), northern

63 (Liang et al., 2022), northeastern (Zhan et al., 2020), and southeastern regions of China

64 (Li et al., 2021; Zeng et al., 2017). These studies suggest considerable increases in Hg

65 in the last century, with the highest Hg flux (70-80 μg m^{-2} yr^{-1}) found in Lake

66 Huguangyan (Li et al., 2021; Zeng et al., 2017) in South China and the lowest (~10 μg

67 m^{-2} yr^{-1}) on the Qinghai-Tibet Plateau (Yang et al., 2010) and in West China (Zeng et

68 al., 2014). However, there are discrepancies between these reconstructions on the

69 evolution trends of Hg pollution and their relations with global Hg emissions derived

70 from the Industrial Revolution. For example, studies from Lake Sayram in West China

71 (Zeng et al., 2014), Lake Gonghai in North China (Liang et al., 2022), Lake Tianchi

72 in Northeast China (Zhan et al., 2020), and Lake Huguangyan in South China (Zeng

73 et al., 2017) reported Hg increases since the late 19th or early 20th century presumably

74 caused by global Hg emissions after the Industrial Revolution, whereas a study (Li et

75 al., 2021) also from Lake Huguangyan and some records (e.g. Cuo Na, Cuo E, Nam

76 Co, and Kemen Co) on the Qinghai-Tibet Plateau (Yang et al., 2010) did not find such

77 increases. In addition, some of the reconstructions only calculated total Hg

78 accumulation rates or enrichment factors (e.g. Kang et al., 2016; Zeng et al., 2017;

79 Zhan et al., 2020), while some calculated anthropogenic Hg accumulation fluxes

80 without considering the focusing effect (e.g. Li et al., 2021; Liang et al., 2022; Zeng

81 et al., 2014). This not only leads uncertainties on revealing evolution trends of

82 anthropogenic Hg in the past but also makes it difficult to conduct comparative

83   analysis of these reconstructions. Until now, it is still unclear about the general

84   variations of atmospheric/anthropogenic Hg in China after the Industrial Revolution

85   and their relations with anthropogenic Hg emissions from developed countries in

86   Europe and North America.

87   In view of this, sediment cores were retrieved from two remote subalpine lakes that

88   were seldom affected by local human activities in North China, and employed to

89   reconstruct historical variations of atmospheric Hg in the past. Based on the records,

90   corrected anthropogenic Hg fluxes in the last two centuries were reconstructed by

91   eliminating the focusing effect. Then, temporal variations and causes of atmospheric

92   Hg pollution were discussed in combination with other pollutants and historical data

93   of economic and industrial developments. Finally, by compiling sediment Hg records

94   over China, historical anthropogenic Hg variations in China and their relation with the

95   global Hg emissions was examined. This study is significant for revealing historical

96   trends of atmospheric Hg in China and understanding global Hg cycling in the

97   industrial era.

98   ## 2. Materials and methods

99   *2.1. Sampling and analysis*

100   Details of the study area, including the two lakes——Lake Gonghai and Lake

101   Mayinghai, are provided in Section S1 of the Supporting Material (SM). Sediment cores

102   were retrieved using a 90-mm diameter gravity corer from the center areas of the lakes.

103   The cores were 60-cm-long for GH from Lake Gonghai and 56-cm-long for MY from

104   Lake Mayinghai. They were sectioned in the field at 1.0 cm interval. The sediment

105   samples were dried at about -40 °C with a vacuum-freezing dryer in the lab, and

106   homogenized and grounded to fine powder (<63 μm) for chemical analyses (Wan et al.,

107   2019a and 2020).

108   Sediment samples were analyzed for ^{137}Cs, ^{210}Pb, and ^{226}Ra by direct gamma assay

109   using a low-background intrinsic germanium detector (EG&G Ortec Gamma

110   Spectrometry) at the State Key Laboratory of Lake Sciences and Environment in China.

111   Chronologies of the cores were calculated using ^{210}Pb and ^{137}Cs radiometric data (Wan

112   et al., 2020). Details of sediment core dating are in Section S2 of the SM.

113   For analyzing element composition, approximately 0.125 g ground sediment was

114   accurately weighted for each sample. Then, it was hot-digested in Teflon digestion tubes

115   with mixed acids of nitric acid, perchloric acid, and hydrochloric acid (Wan et al., 2016).

116   After digestion, the samples were diluted to 50 ml with double-distilled deionized water.

117   Then, the solutions were taken for determining concentrations of major elements such

118   as Al, Ti and Ca in both GH and MY sediments by a Leeman Labs Profile inductively

119   coupled plasma atomic emission spectrometry (ICP-AES) and trace elements including

120   Cd, As and Pb in GH sediments by an Agilent 7700x inductively coupled plasma mass

121   spectrometry (ICP-MS) at the State Key Laboratory of Lake Sciences and Environment

122   (Wan et al., 2019a). The precision of these measurements was less than 5% for their

123   relative standard deviations.

124   Mercury measurements for the GH sediments were conducted at Environment

125 Research Center in University College London following the method of Yang et al

126 (2016). Briefly, the sediment was firstly digested using 8 mL of aqua regia on a hot

127 plate at 100 °C for 1.5 h in 50 mL polypropylene DigiTUBE (SCP Science). Then,

128 mercury concentrations in the digested solutions were analyzed using a cold vapor-

129 atomic fluorescence spectrometry (CV-AFS) following reduction with $SnCl_2$. Quality

130 control was conducted by digesting and analyzing analytical blanks and standard

131 reference materials (stream sediment GBW07305, certified Hg value 100 ± 10 ng g^{-1}).

132 The average recovery rates of Hg were 93±8% for the reference material of GBW07305.

133 Mercury concentrations in the MY sediments were measured using a direct mercury

134 analyzer (Hydra-C, Leeman Labs Inc) following the USEPA method at the State Key

135 Laboratory of Lake Sciences and Environment (Wan et al., 2022). Standard reference

136 material (GSD-23) and duplicate measurements were employed to control the analysis

137 quality. The measurement errors were less than 5%, with a detection limit of 0.6 ng g^{-1}.

138 　　Analytical details for other parameters including grain-size composition, contents

139 of total organic carbon (TOC), total nitrogen (TN), and diatom assemblages can be

140 found in Section S3 of the SM.

141 *2.2. Calculation of anthropogenic Hg flux*

142 　　To reflect human-derived Hg trends, anthropogenic Hg fluxes were estimated in

143 the two sediment cores. The anthropogenic Hg flux (Hg[$Flux_{anthr}$], µg m^{-2} yr^{-1}) was

144 calculated by the following equation (Wan et al., 2019b):

145 Hg[$Flux_{anthr}$] = (Hg[C_{sample}] − Hg[$C_{background}$] × R[C_{sample}] / R[$C_{background}$]) × SR × ρ × 10

146   (2)

147   where Hg[C_{sample}] and Hg[$C_{background}$] represent Hg concentrations in sediment samples

148   and in background sediment, respectively. R[C_{sample}] and R[$C_{background}$] represent Ti

149   concentrations in sediment samples and in background sediment, respectively. SR

150   represents sedimentation rate (cm yr^{-1}) and ρ is dry bulk density (g cm^{-3}) of the sediment.

151   For a few sediment samples in the lower core section without Ti measurement (GH: 42,

152   48, 52, and 60 cm; MY: 33, 37, 40, 46, and 55 cm), background Ti or average Ti values

153   in their upper and lower samples were taken for the calculation. Negative values of the

154   calculated flux in the background sections of the sediment cores were set to zero.

155   Finally, the anthropogenic Hg flux was corrected for the influence of sediment

156   focusing by using the following equations (Perry et al., 2005):

157   Hg[$Flux_{anthr}$]$_c$ = Hg[$Flux_{anthr}$]/F   (3)

158   F = $(\sum F^{210}Pb_{ex, core})/(\sum F^{210}Pb_{ex, regional})$ (4)

159   where $\sum F^{210}Pb_{ex, local}$ represents unsupported ^{210}Pb inventory measured in the sediment

160   core, and $\sum F^{210}Pb_{ex, regional}$ represents the regional $^{210}Pb_{ex}$ reference inventory in this

161   region. The regional $^{210}Pb_{ex}$ reference inventory referred to the value of 5730 Bq m^{-2}

162   revealed by (Zhang et al., 2003) in adjacent province of Shaanxi with similar

163   precipitations to that of the study lakes.

164   **3. Results and discussion**

165   **3.1. Historical variations of anthropogenic Hg in GH and MY**

166   **3.1.1. Anthropogenic Hg variations before ~1950**

167   In the period of 1780s-1950, Hg concentrations in the GH core had a range of 17.1-

168   23.2 ng g^{-1}, with an average of 19.5±2.2 ng g^{-1}; while those in the MY core had a range

169   of 35.8-42.8 ng g^{-1}, with an average of 39.6±2.1 ng g^{-1}. The average Hg concentration

170   in GH was only half of that in MY, which could be ascribed to relatively low

171   background Hg in soil in Lake Gonghai catchment compared to Lake Mayinghai.

172   Although the large differences, Hg concentrations in the two sediment cores were

173   relatively low and stable during this period (Fig. 1). After ~1950, Hg concentrations in

174   the two sediment cores increased rapidly. In the 2010s, Hg concentration in GH reached

175   64.5 ng g^{-1}, increased by a factor of three as against that in 1780s-1950; while that in

176   MY reached 66.4 ng g^{-1}, increased by a factor of nearly two.

177   Mercury concentrations in lake sediments are usually affected by both

178   anthropogenic emissions and natural factors such as lake sedimentation rate, primary

179   productivity, and terrigenous detrital inputs (Cooke et al., 2020). To help distinguish

180   anthropogenic and natural contributions, anthropogenic Hg fluxes were reconstructed

181   and corrected in the two records.

182   In the 1780s-1950, the corrected anthropogenic Hg fluxes in GH and MY cores

183   were close to zero (Fig. 1). Although there were several fluctuations in the fluxes during

184   this period, e.g. peaks in the 1860s in GH and in the 1820s in MY, they all were

185   relatively minor compared to the increases in recent decades (Fig. 1) and it is difficult

186   to determine whether they were related to real anthropogenic influence or natural

187   fluctuation. These data suggest that the reconstructed anthropogenic Hg fluxes, similar

188   to Hg concentrations, were relatively low and stable in 1780s-1950, indicating

189   negligible contribution of anthropogenic Hg.

190   In addition, sedimentary compositions, including grain sizes, Al, Ti, and Ca, of the

191   two sediment cores only showed slight variations in this period (Fig. 2), suggesting

192   relatively stable sedimentation environments in the two lakes. This provided good

193   sedimentation backgrounds for faithfully recording anthropogenic Hg pollution signals,

194   further implying that the low and stable Hg fluxes could reflect the negligible

195   anthropogenic Hg signals in this period.

196   Liang et al. (2022) also reconstructed historical Hg variations in GH and MY using

197   sediment cores. The study reported similar negligible anthropogenic Hg signals before

198   ~1950 in Lake Mayinghai but an earlier increase in anthropogenic Hg since the late

199   19th century in Lake Gonghai (Fig. 3) (Liang et al., 2022). From the comparison of Hg

200   concentration *vs* depth in GH and MY between our study and Liang et al. (2022), it can

201   be seen that vertical variations of Hg concentrations in the two studies fitted well with

202   each other and sharp increases in Hg concentrations occurred in similar upper core

203   sections (Fig. 3). This suggests the reliability of sampling and measurement in the two

204   studies and that their discrepancy was caused by sediment core dating.

205   For vertical variations of ^{137}Cs in GH (Fig. 3), our study and Liang et al. (2022)

206   both showed the first occurrence of ^{137}Cs at 24-25 cm depth and the first peak at 20-21

207   cm. Increases of ^{137}Cs from 25 to 20 cm depth were sharp, without any trailing

208   phenomenon. This suggests that the depth of 24-25cm probably corresponded to the

209   early 1950s when nuclear tests started to increase worldwide and that the depth of 21cm

corresponded to the early 1960s when nuclear tests peaked. These deduced ages fit well with our dating results of GH core, but show a half-century discrepancy compared to that of GH core in Liang et al. (2022). If the GH core in Liang et al. (2022) was in line with this ^{137}Cs ages, its temporal variation of Hg would be in agreement with the record in their MY core and our two records in this study.

The dating results of the MY cores in our study and Liang et al. (2022) showed similar ages for the ^{137}Cs peak of 1963 (Fig. 3). And the two studies reported almost the same temporal variations of Hg in MY. In addition, our reconstruction shows similar Hg fluxes between the two lakes, whereas that of Liang et al. (2022) shows large discrepancy in fluxes between the two lakes (Fig. 3). These facts suggest the reliability of our dating and reconstructions, confirming the negligible anthropogenic Hg signals in the lakes before ~1950.

3.1.2. Rapid increases in atmospheric Hg since the 1950s

Since the 1950s, the corrected anthropogenic Hg fluxes, similar as Hg concentrations, have begun to increase rapidly in the two records (Fig. 1). Heavy-metal increases in recent lake sediments usually relate to increased atmospheric deposition, direct dumping into the lakes, and variations of aquatic primary productivity and catchment erosion (Yang, 2015; Wan et al., 2020). Lakes Gonghai and Mayinghai are situated remotely in the Lvliang Mountains. There was no industry around the lakes. Although TOC content in the GH core experienced a rapid increase during ~1970-1990 (Fig. 4), the primary productivity in the lake did not experience obvious changes until

231 ~1985 indicated by diatom changes (Fig. 4). This time was significantly later than the

232 major Hg increase occurred in ~1950-1990. Corrected anthropogenic Hg fluxes in MY

233 also increased significantly during 1950-1990, but TOC and TOC/TN did not change

234 much in this period (Fig. 4) (Liang et al., 2022). These suggest that the recent Hg

235 increases in the two lakes had little relation with the aquatic primary productivity.

236 Finally, the two lakes might receive a certain amount of anthropogenic Hg from their

237 catchment via erosion (Liang et al., 2022). However, the amount was likely not large,

238 considering that the lakes are located on a semi-arid climate area with a mean annual

239 precipitation of only 468 mm and they have relatively low catchment/lake area ratios

240 (2-6) as they are known as Tianchi (crater lake) situated on mountain tops. A study in

241 semi-arid lakes on the Tibetan Plateau estimated that contribution of Hg caused by

242 catchment input accounted for no more than ~11% of the total Hg in the lake sediments

243 (Yang et al., 2010). In addition, as atmospheric Hg in China did not experience obvious

244 declines in recent decades (Tian et al., 2015), the fractions of the atmospheric Hg fluxes

245 which have been transported to the lake from the catchment should be relatively

246 constant (Yang et al., 2015). These suggest that the Hg increases in recent several

247 decades in the two sediment cores were mainly related to atmospheric deposition.

248   In 1950-2014, the maximum Hg concentration in GH increased by 3.4 times

249 compared with the background value, while that in MY increased only by 85% (Fig. 1).

250 Although the two records have large discrepancies in Hg concentration, they show

251 similar corrected anthropogenic Hg fluxes and evolution trends. This indicates that the

252 two lakes had been affected by the same source——regional atmospheric deposition,

253   and thus they could be used to reflect atmospheric mercury variations in the past.

254   Since the 1950s, the anthropogenic Hg fluxes in both cores had increased

255   significantly, suggesting a rapid increase in atmospheric Hg level in the region. This

256   change corresponded well to the rapid development of economy and industry in the

257   region after the founding of the PR China in 1949. Shanxi province and its surrounding

258   areas, rich in coal and steel resources, were a key development area in industry in the

259   early years of New China (Liu, 2009). In the 1950s, there were eight key constructive

260   industrial cities in the whole China, with three of them situated in the region, i.e.

261   Taiyuan (~120 km south to the lakes), Datong (~150 km northeast), and Baotou (~270

262   km northwest) (Zhou, 2005). The backward trajectories show that these cities are

263   located on the main directions of atmospheric circulation over the lakes (Fig. S3).

264   In the early period of New China, heavy industry, especially iron and steel, was the

265   top priority of economic development. In 1949, annual production of cast iron in Shanxi

266   Province was only 40,000 tons. However, in 1960 it reached 1.19 million tons,

267   increased by nearly 30 times (Fig. 5) (SBSP, 1999). In 1958-1960, there even occurred

268   a nationwide campaign to make iron and steel. In this period, most of the iron and steel

269   refining furnaces were small and crude, with less developed technology and poor

270   management (EBFYCISI, 1999). The output of iron and steel was relatively low, but

271   the pollutant emissions were high, which caused rapid increase in atmospheric Hg

272   emissions in the region. The increase trend of Hg since the 1950s in GH and MY

273   sediments was consistent with estimated atmospheric Hg emissions in China (Fig. S4)

274   (Tian et al., 2015) and synchronous with the sediment records from most regions of

275   China (Li et al., 2021; Liu et al., 2015; Yang et al., 2010).

276   In the late 1990s, the anthropogenic Hg fluxes in the two cores experienced an

277   obvious decrease, suggesting a decline in atmospheric Hg level in this region. In 1997,

278   the Asian financial crisis triggered a national economic recession in China. Coal and its

279   related industries entered a downturn period, as coal price continued to fall despite

280   rising production cost. As an important province of coal production and consumption,

281   annual coal consumption in Shanxi Province changed from a rapid rise in the early

282   1990s to a decline in 1997-2001 (Fig. 5)

283   (http://calendar.hexun.com/area/dqzb_140000.shtml). This change caused a decrease in

284   pollutant emissions in the region, corresponding to the decline in atmospheric Hg level.

285   These imply that the two sediment cores may have recorded the regional atmospheric

286   Hg changes in the past.

287 3.2. Comparison with historical variations of other pollutants in the
288 lakes

289   From historical variations of other pollutants, including other heavy metals, black

290   carbon, and PAHs, in these lakes (Fig. 6), heavy metals and PAHs concentrations were

291   also relatively low and stable during 1780s-1950. Only black carbon experienced some

292   slight rises (e.g. in the 1870s in Lake Mayinghai, in the 1930s in Lake Gonghai), which

293   were probably caused by natural factors like wildfires rather than human-related

294   emissions (Zhan et al., 2019). This suggests that the lakes were seldom affected by not

295   only anthropogenic Hg but also other pollutants before 1950.

296   Since the 1950s, black carbon and PAHs showed similar increasing trend with Hg,

297   but other heavy metals did not increase till ~1980 AD. This was probably because that

298   heavy metals are usually transported shorter distance in the atmosphere than Hg as they

299   tend to stick to atmospheric particulates (Lü et al., 2019). Heavy metals in the lakes

300   were affected by pollutant emissions mainly from nearby cities such as Ningwu,

301   Shenchi, and Wuzhai, where industry developed later and development level was

302   relatively low in Shanxi Province (Peng et al., 2010).

303   3.3. Comparison with Hg records from other regions

304   Since the beginning of the Industrial Revolution in the 1860s, global

305   anthropogenic Hg emissions have increased rapidly due to fossil fuel combustion,

306   mining, and industrial production (Hylander and Meili, 2003; Streets et al., 2019).

307   Model estimations suggest that the global atmospheric Hg emissions in the late 19th

308   century reached ~2500 ton yr^{-1}, only slightly lower than that in the 1960s (Fig. S4)

309   (Streets et al., 2019). Similarly, many sediment records from Europe and North America

310   also show considerable increases in anthropogenic Hg since the late 20th century (e.g.

311   Cooke et al., 2020; Corella et al., 2017; Cortizas et al., 2012).

312   In China, some studies (Fig. 7), such as Lake Huguangyan Marr in South China

313   (Zeng et al., 2017), lakes of Qinghai, Keluke, and Gahai on the Qinghai-Tibet Plateau

314   (Yang et al., 2010), Lake Tianchi in Northeast China (Zhan et al., 2020), and Badain

315   Jaran Desert (Liu et al., 2015), reported earlier increases in Hg since the late 19th

316   century and inferred those were likely caused by global industrial Hg emissions.

317   However, from their trends in Fig. 7, it can be seen that most of these Hg increases were

318 not obvious before ~1950 compared to their recent and even early natural changes.

319 Together with that most of previous studies did not calculate historical anthropogenic

320 Hg contributions (Kang et al., 2016; Liu et al., 2015; Zeng et al., 2017; Zhan et al., 2020)

321 and investigated only one single sediment core without any comparative ones (Li et al.,

322 2021; Liu et al., 2015; Zeng et al., 2014 and 2017; Zhan et al., 2020), there are still

323 uncertainties on the inference of these Hg increases related to global Hg emissions.

324 Our records of historical Hg variations in GH and MY suggested negligible

325 increases in anthropogenic Hg before ~1950 (Fig. 1). Besides, some other sediment

326 records from China that calculated anthropogenic Hg contributions, e.g. Lake

327 Huguangyan Marr in South China (Li et al., 2021) and lakes of Cuo Na, Cuo E, Nam

328 Co, and Kemen Co on the Qinghai-Tibet Plateau (Yang et al., 2010), also showed

329 similar negligible increases in Hg before ~1940-1950 (Fig. 7). These negligible

330 anthropogenic Hg signals indicate that the above Hg increases in the late 19th and early

331 20th centuries could not be caused by long-range transport and deposition of the global

332 Hg emissions, as atmospheric deposition at the global scale should cause similar Hg

333 pollution signals in all lake sediment records with similar Hg backgrounds in China. It

334 is known that the early global Hg emissions were contributed mainly (~80% in 1880s-

335 1890s and ~50-60% in 1900-1950) by developed countries in Europe and North

336 America (Streets et al., 2019) which are situated the farthest away from China in the

337 Northern Hemisphere. Some of them may have been transported and deposited into

338 remote China, but they were likely not enough to leave obvious signals in most

339 sediment records. Even in Eastern America (Rhode Island), a lake sediment record

340   showed little indication of increased Hg deposition related to the late 19th-century silver

341   and gold mining in the western USA (Fitzgerald et al., 2018). Therefore, obvious

342   anthropogenic Hg signals occurred in some lake sediment records in China before 1950

343   should be more likely ascribed to local/regional Hg sources than global emissions. For

344   example, in Lake Sayram in West China (Zeng et al., 2014) and three lakes in

345   southeastern Inner Mongolia (Wan et al., 2022) in North China, considerable increases

346   in anthropogenic Hg were found in the first half of the 20th century, and they both were

347   speculated to be caused by regional emissions.

348   Although the Hg records in China exhibit differences in their early Hg changes

349   before the 1950s, most of them show significant Hg increases since the 1950s related

350   to Hg emissions in China (Li et al., 2021; Liu et al., 2015; Yang et al., 2010; Zhan et al.,

351   2020) (Fig. 7). The change fitted well with the backward industry in old China and

352   quick developments of industry after the founding of the PR China in 1949. The model

353   estimated atmospheric Hg emission in China was only ~12.5 ton yr^{-1} in the year of

354   ~1950 (Tian et al., 2015), which was only ~1/10 of that in Asia (131 ton yr^{-1}) and ~1/100

355   of the global emissions (1330 ton yr^{-1}) (Streets et al., 2019). In 1959, the emission

356   increased rapidly to ~270 ton yr^{-1} (Tian et al., 2015), which was 21.6 times of that in

357   ~1950. The above facts indicate widespread increases in atmospheric Hg in China likely

358   occurred after the founding of New China, obviously later than the beginning time of

359   the Industrial Revolution. The finding supports assessments that most of the 20th

360   century Hg emissions were deposited locally near urban and industrial centers of Hg

361   use and release (Cooke et al., 2022; Fitzgerald et al., 2018). However, it should be noted

362 that most of the above Hg records were usually of uncertainties on core dating and

363 affected by local Hg sources at different degrees, the exact increase time in atmospheric

364 Hg and its spatial variations should be further studied by investigating more reliable

365 sediment records from different regions in China.

366

367 **4. Conclusions**

368 In this study, historical variations in atmospheric Hg over the last two centuries were

369 reconstructed using two sediment cores from remote lakes in Shanxi Province in North

370 China. Compared with the background, the present Hg concentration in the GH core

371 increased by ~3 times, whereas that in the MY core increased by only 85%, ascribed to

372 relatively low background Hg in catchment soil in Lake Gonghai compared to Lake

373 Mayinghai. Despite of the large difference in Hg concentrations between the two cores,

374 their corrected anthropogenic Hg fluxes were close and showed similar evolution trends.

375 The two records show relatively low and stable anthropogenic Hg fluxes in the whole

376 19th and the first half of the 20th centuries, suggesting negligible pollution signals of

377 atmospheric Hg. The fact indicates little influence of early industrial Hg emissions,

378 which was likely caused by that the early Hg emissions were contributed mainly by

379 developed countries in Europe and North America and that few of them were

380 transported and deposited into remote China. Rapid increases in atmospheric Hg in this

381 region have occurred since the 1950s, derived mainly from regional Hg emissions. This

382 corresponded well with the rapid development of industry in and around Shanxi

383 Province after the founding of the PR China. The results imply a possible minor

384 influence of Hg emissions dominated by Europe and North America in the late 19th and

385 early 20th centuries on China. The findings are significant for understanding historical

386 variations of atmospheric Hg in China and the influence of the early industrial Hg over

387 the globe.

388

Ethical Approval

390   Not applicable.

Consent to Participate

392   Not applicable.

Consent to Publish

394   Not applicable.

Authors Contributions

396   Dejun Wan: Conceptualization, Data curation, Formal analysis, Investigation,

397 Methodology, Project administration, Software, Visualization, Writing original draft.

398 Handong Yang: Supervision, Validation, Writing - review & editing. Zhangdong Jin:

399 Funding acquisition, Supervision, Writing - review & editing. Lei Song: Investigation,

400 Methodology, Supervision, Review & editing. Dongliang Ning, Longjuan Cheng, and

Qingfeng Jiang: Methodology and Review & editing.

Funding

Competing Interests

Not applicable.

Availability of data and materials

All data generated or analyzed during this study are included in this published article.

Acknowledgements

Appendix A. Supplementary data

Supplementary data to this article can be found in *Supporting Material*.

References

Appleby, P.G., 2001. Chronostratigraphic Techniques in Recent Sediments-Tracking Environmental Change Using Lake Sediments. Springer, Netherlands, 171–203.

Cooke, C.A., Martínez-Cortizas, A., Bindler, R., Gustin, M.S., 2020. Environmental archives of atmospheric hg deposition – a review. Science of The Total Environment, 709, 1-15.

Corella, J.P., Valero-Garcés, B.L., Wang, F., Martínez-Cortizas, A., Cuevas, C.A., Saiz-Lopez, A., 2017. 700 years reconstruction of mercury and lead atmospheric deposition in the Pyrenees (NE Spain). Atmospheric Environment, 155, 97-107.

Cortizas, A.M., Varela, E.P., Bindler, R., Biester, H., Cheburkin, A., 2012. Reconstructing historical Pb and Hg pollution in NW Spain using multiple cores from the Chao de Lamoso bog (Xistral Mountains). Geochimica et Cosmochimica Acta 82, 68–78.

Dai, A., Yan, J., 2000. Geographical distribution, change and impact of modern industry in China. Essays on Chinese Historical Geography 1, 139-251 (In Chinese).

EBFYCISI (Editorial Board of Fifty Years of Chinese Iron and Steel Industry), 1999. Fifty years of Chinese steel industry. Beijing: Metallurgical Industry Press, 108-197.

Fitzgerald, W.F., Engstrom, D.R., Hammerschmidt, C.R., Lamborg, C.H., Balcom, P.H., Lima-Braun, A.L., Bothner, M.H., Reddy, C.M. Global and Local Sources of Mercury Deposition in Coastal New England Reconstructed from a Multiproxy,

439   High Resolution, Estuarine Sediment Record. Environ. Sci. Technol. 2018, 52,

440   7614−7620.

441   Driscoll, C.T., Mason, R.P., Chan, H. M., Jacob, D.J., Pirrone, N., 2013. Mercury as a

442   global pollutant: sources, pathways, and effects. Environmental Science &

443   Technology, 47(10), 4967-4983.

444   Fu, X., Zhang, H., Yu, B., Wang, X., Lin, C., Feng, X., 2015. Observations of

445   atmospheric mercury in China: a critical review. Atmospheric Chemistry and

446   Physics, 15(16), 9455-9476.

447   Hylander L.D. and Meili M., 2003. 500 years of mercury production: global annual

448   inventory by region until 2000 and associated emissions. Science of the Total

449   Environment, 304(1-3), 13-27.

450   Kang S., Jie H., Wang F., Zhang Q., Guo J., 2016. Atmospheric mercury depositional

451   chronology reconstructed from lake sediments and ice core in the Himalayas and

452   Tibetan Plateau. Environmental Science & Technology, 50(6),

453   10.1021/acs.est.5b04172.

454   Li T., Zhong W., Wei Z., Shang S., Ye S., Chen, Y., et al., 2021. Response of mercury

455   accumulation to anthropogenic pollution in the past 1000 years based on Lake

456   Huguangyan sediments, Southern China. Environmental Geochemistry and

457   Health, 1-13, doi.org/10.1007/s10653-021-00878-2.

458   Liang, M., Liu, E., Wang, X., Zhang, Q., Xu, J., Ji, M., Zhang, E., 2022. Historical

459   trends in atmospheric metal(loid) contamination in North China over the past

460   half-millennium reconstructed from subalpine lake sediment. Environmental

461   Pollution, 304, 119195, doi.org/10.1016/j.envpol.2022.119195.

462   Liu Y., 2009. Study of the 60-year development of Shanxi as an energetic and old

463   industrial base. Academic Journal of Shanxi Provincial Committee Party School

464   of C.P.C, 32 (6), 51-53 (In Chinese with English abstract).

465   Lü, H., Huang, Y., Huang, X., Cai, Q., 2019. The state of particulate matter (PM)

466   contamination, PM -bound heavy metals and persistent organic pollutants (POPs)

467   in megacities, China. Current Opinion in Environmental Science & Health, 8, 15-

468   22.

469   Ma, Z., Hu, X., Sayer, A.M., Levy, R., Zhang, Q., Xue, Y., Tong, S., Bi, J., Huang, L.,

470   Liu, Y., 2016. Satellite-based spatiotemporal trends in PM2.5 concentrations:

471   China, 2004–2013. Environ. Health Perspect. 124, 184–192.

472   Peng F., Han Z., Ma H., 2010. Analysis on differences and causes of regional economic

473   development in Shanxi Province in the last 15 years. Areal Research and

474   Development, 29 (6), 12-17 (In Chinese with English abstract).

475   SBSP (Statistics Bureau of Shanxi Province), 1999. Statistical Yearbook of Shanxi

476   Province. China Statistics Press, Beijing (In Chinese).

477   Streets D., Horowitz H.M., Lu Z., Levin L., Thackray C.P., Sunderland E.M., 2019.

478   Five hundred years of anthropogenic mercury: spatial and temporal release

479   profiles. Environmental Research Letters, 14, 084004, doi.org/10.1088/1748-

480   9326/ab281f.

481   Tian H., Zhu C., Gao J., Cheng K., Hao J., Wang K., et al., 2015. Quantitative

482   assessment of atmospheric emissions of toxic heavy metals from anthropogenic

483   sources in China: historical trend, spatial distribution, uncertainties, and control

484   policies. Atmospheric Chemistry and Physics, 15(17), 10127-10147.

485 UNEP (United Nations Environment Programme), 2018. Global Mercury Assessment

486   2018. Narayana Press, Gylling, Denmark.

487 Wan, D., Song, L., Yang, J., Jin, Z., Zhan, C., Mao, X., Liu, D., Shao, Y., 2016.

488   Increasing heavy metals in the background atmosphere of central North China

489   since the 1980s: evidence from a 200-year lake sediment record. Atmospheric

490   Environment, 138, 183-190.

491 Wan D, Mao X, Jin Z, Song L, Yang J, Yang H, 2019a. Sedimentary biogeochemical

492   record in Lake Gonghai: implications for recent lake changes in relatively remote

493   areas of China. Science of the Total Environment, 649, 929-937.

494 Wan D, Song L, Mao X, Yang J, Jin Z, Yang H, 2019b. One-century sediment records

495   of heavy metal pollution on the southeast Mongolian Plateau: implications for air

496   pollution trend in China, Chemosphere, 220, 539-545.

497 Wan D., Yang H., Jin Z., Xue B., Song L., Mao X., Yang J., 2020. Spatiotemporal trends

498   of atmospheric Pb over the last century across inland China. Science of the Total

499   Environment 729, 138339, doi.org/10.1016/j.scitotenv.2020.138399.

500 Wan, D., Yang, H., Song, L., Jin, Z., Mao, X., Yang, J., 2022. Sediment records of global

501   and regional Hg emissions to the atmosphere in North China over the last three

502   centuries.   Environmental   Pollution,   310,   119831,

503   doi:10.1016/j.envpol.2022.119831.

504 Wu Q., Wang S., Li G., Liang S., Lin C. J., Wang Y., et al., 2016. Temporal trend and

505   spatial distribution of speciated atmospheric mercury emissions in China during

506   1978–2014. Environmental Science & Technology, 50(24), 13428-13435.

507 Yang, H., 2015. Lake Sediments May Not Faithfully Record Decline of Atmospheric

508   Pollutant Deposition. Environmental Science & Technology, 49, 12607-12608.

509 Yang, H., Battarbee, R.W., Turner, S.D., Rose, N.L., Derwent, R.G., Wu, G., Yang, R.,

510   2010. Historical reconstruction of mercury pollution across the Tibetan Plateau

511   using lake sediments. Environmental Science & Technology, 44(8), 2918-2924.

512 Yang, H., Turner, S., Rose, N.L. 2016. Mercury pollution in the lake sediments and

513   catchment soils of anthropogenically-disturbed sites across England.

514   Environmental Pollution. 219: 1092-1101.

515 Zeng H., Wu J., Liu W., 2014. Two-century sedimentary record of heavy metal pollution

516   from Lake Sayram: A deep mountain lake in central Tianshan, China. Quaternary

517   International 321, 125-131.

518 Zeng Y., Chen J., Yang Y., Wang J., Zhu Z., Li J., 2017. Huguangyan Maar Lake (SE

519   China): A solid record of atmospheric mercury pollution history in a non-remote

520   region. Journal of Asian Earth Sciences, 147, 1-8.

521 Zhan C, Wan D, Han Y, Zhang J, 2019. Historical variation of black carbon and PAHs

522   over the last similar to 200 years in central North China: Evidence from lake

523   sediment records. Science of the Total Environment 690, 891-899

524 Zhan T., Zhou X., Cheng W., He X., Tu L. Liu X., Ge J., Xie Y., Zhang J., Ma Y., Li E.,

525   Qiao Y., 2020. Atmospheric mercury accumulation rate in northeastern China

526   during the past 800 years as recorded by the sediments of Tianchi Crater Lake.

527   Environmental Science and Pollution Research, 27(1), 571-578.

528   Zhang, X., Walling, D.E., Feng, M., Wen, A., 2003. $^{210}Pb_{ex}$ depth distribution in soil

529   and calibration models for assessment of soil erosion rates from $^{210}Pb_{ex}$

530   measurements. Chinese Science Bulletin, 48(8), 813-818.

531   Zhou M., 2005. Study on the strategy of heavy industry priority development and

532   industry city development during the initial stage of New China. Sichuan

533   University, master dissertation, 51-57 (In Chinese with English abstract).

534

535
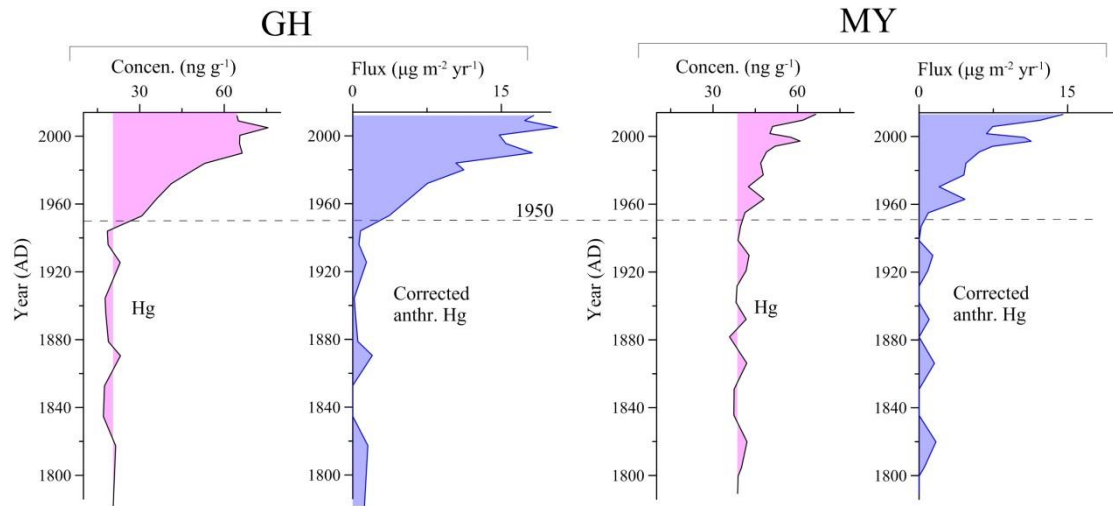
Fig. 1 Temporal variations of Hg concentrations and corrected anthropogenic Hg fluxes

in GH and MY.

539
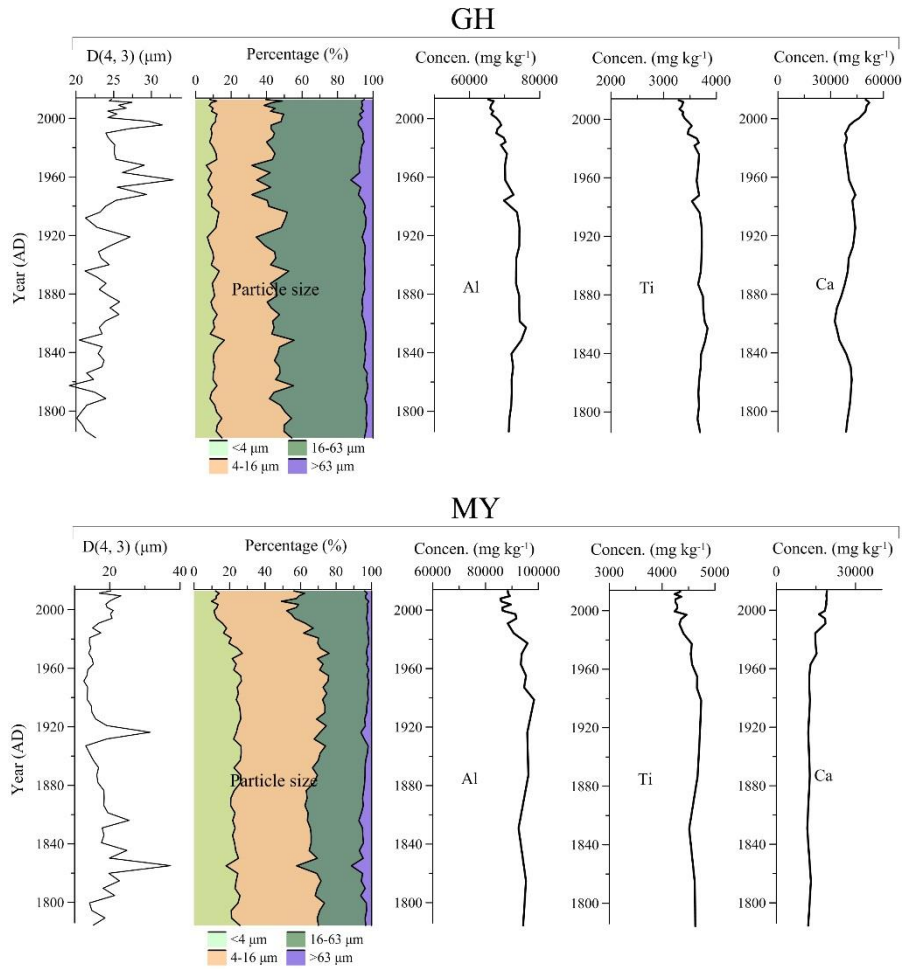
Fig. 2 Temporal variations of grain sizes, Al, Ti, and Ca in the two sediment cores. D

541   (4, 3) and percentage (%) represent volume-weighted mean grain size and relative

542   percentage of each component of grain size in sediment, respectively.
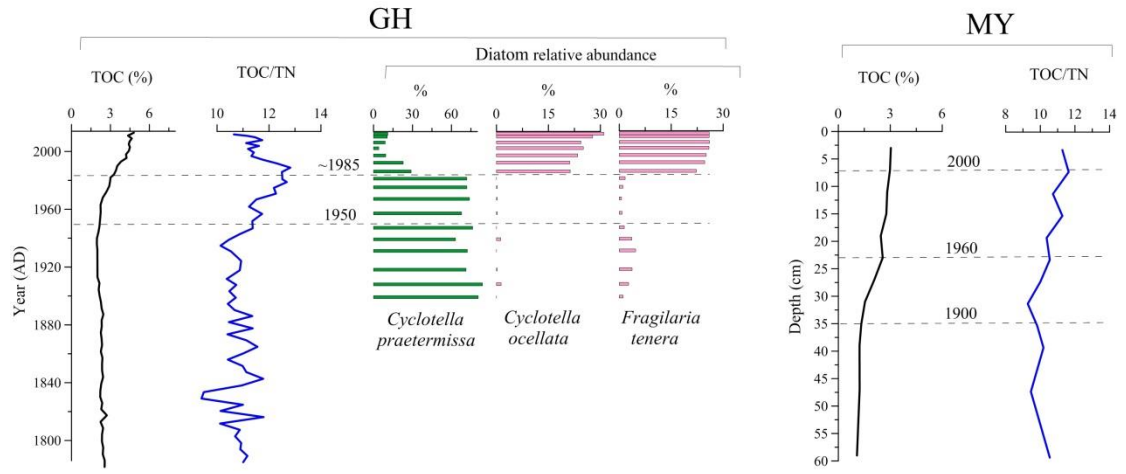
543

544
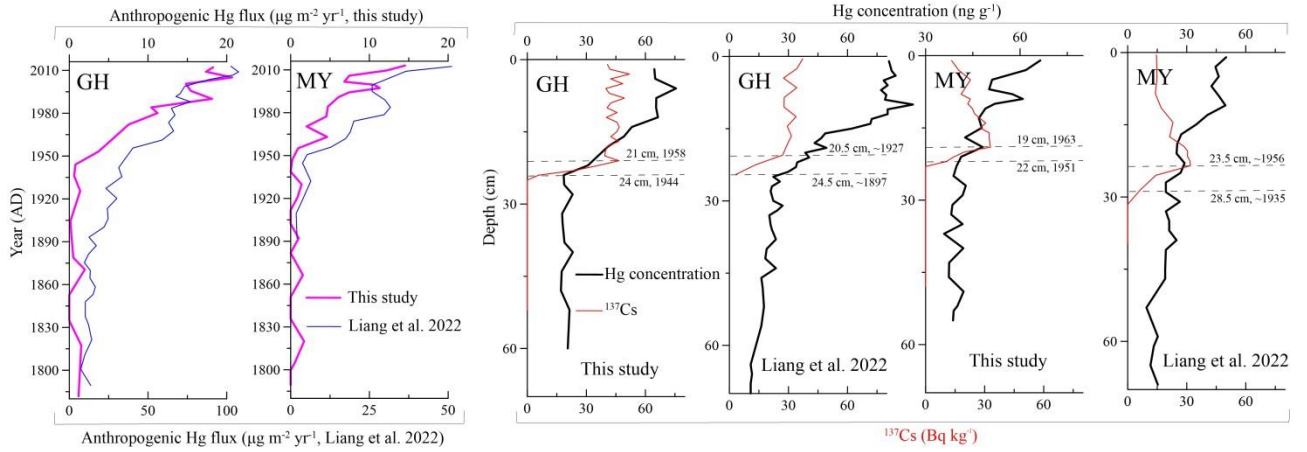
Fig. 3 Comparisons of reconstructed anthropogenic Hg fluxes, Hg concentrations, and

546   [137]Cs in the two lakes between this study and Liang et al. (2022).

547

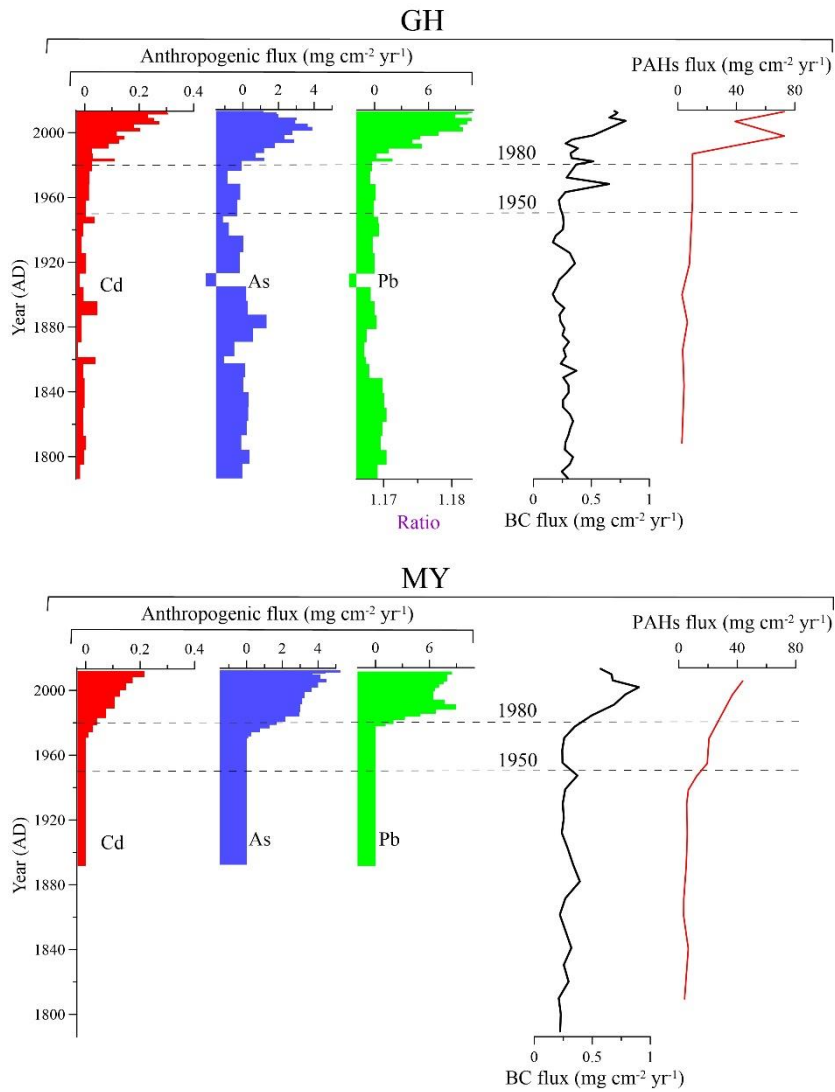**Fig. 4** Temporal trends of TOC, TOC/TN, and diatom in GH and MY. Data of TOC and TOC/TN in MY were from Liang et al. (2022).

552
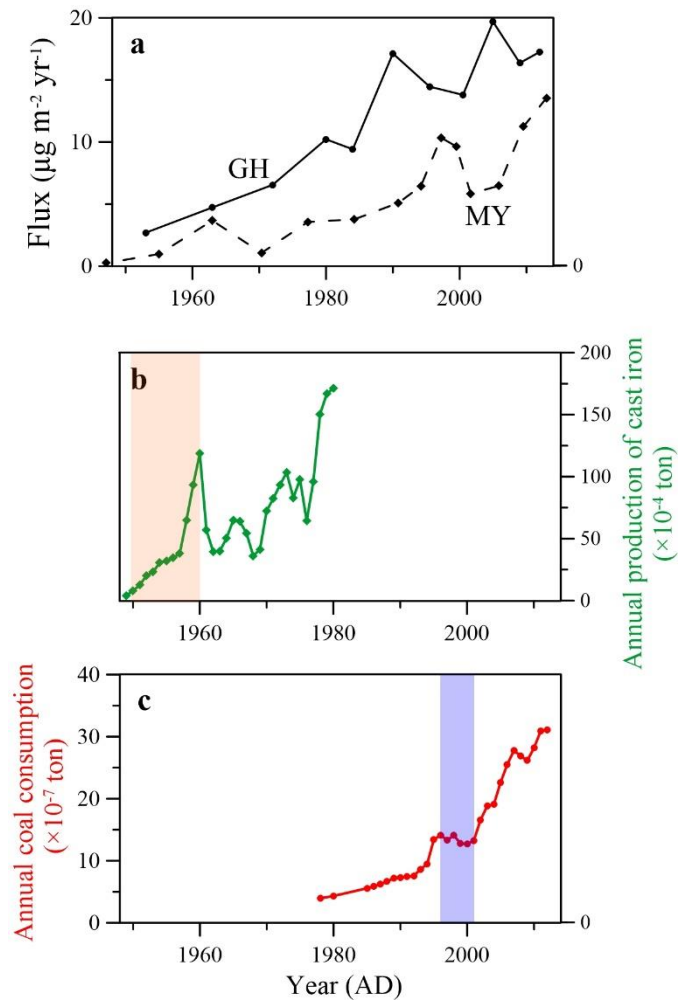
Fig. 5 (a) Corrected anthropogenic Hg fluxes in GH and MY in 1949-2014, (b) annual

production of cast iron (SBSP, 1999), and (c) coal consumption in Shanxi Province

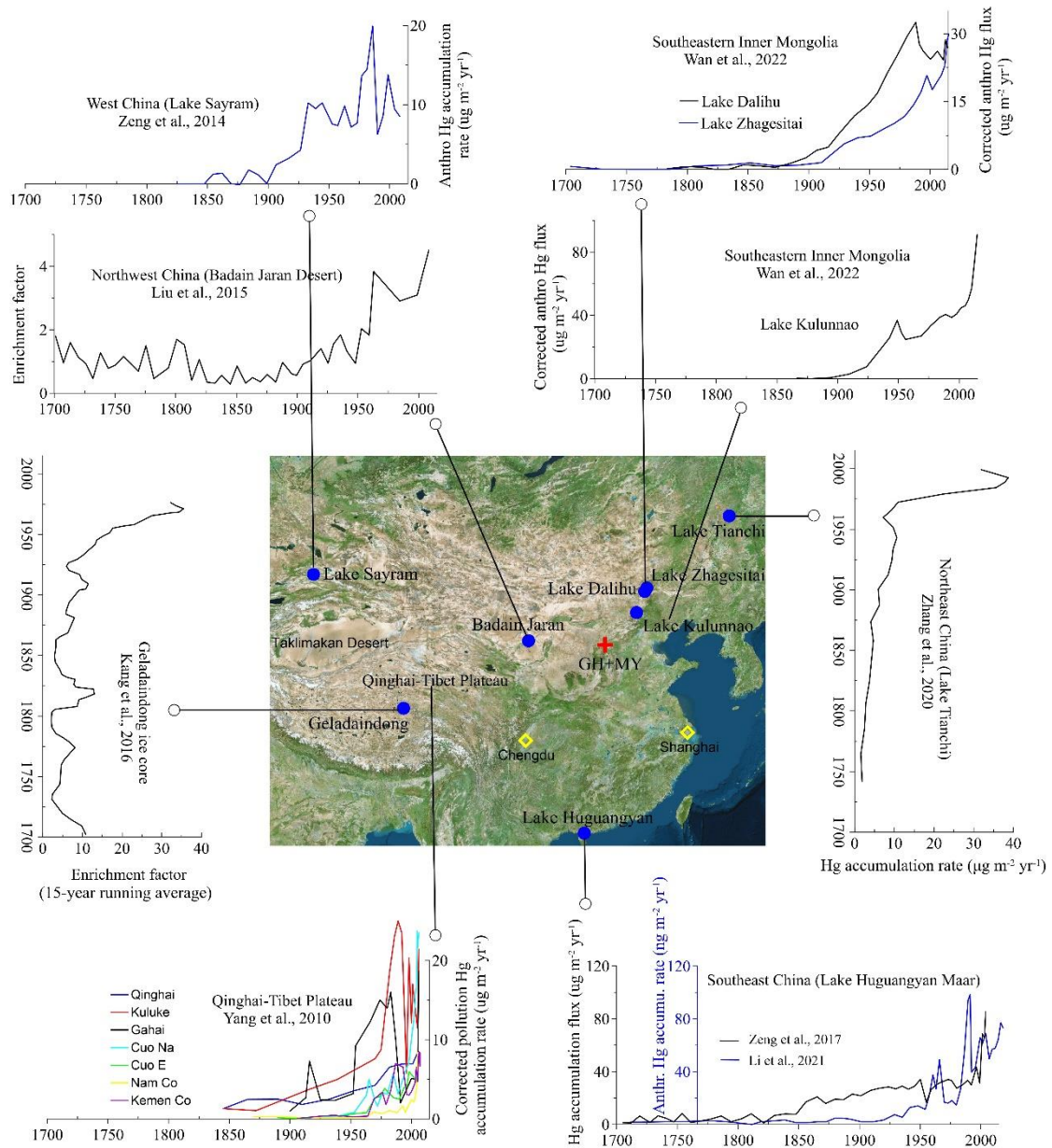(http://calendar.hexun.com/area/dqzb_140000.shtml). 坐标轴没对齐。

556

557

Fig. 6 Historical variations of reconstructed heavy metals, BC, and PAHs fluxes in lake

sediment cores of GH and MY. Data sources: BC and PAHs from Zhan et al. (2019),

and heavy metals in Lake Mayinghai from Liang et al. (2022).

561

562

Fig. 7 Comparisons with Hg records from other regions in China, including Lake Tianchi in Northeast China (Zhan et al., 2020), three lakes in southeastern Inner Mongolia (Wan et al., 2022), Lake Huguangyan Maar in South China (Li et al., 2021; Zeng et al., 2017), a small lake in Badain Jaran Desert in Northwest China (Liu et al., 2015), Lake Sayram in West China (Zeng et al., 2014), and Geladaindong ice core (Kang et al., 2016) and seven lakes (Yang et al., 2010) on the Qinghai-Tibet Plateau.

加北京、玛珥湖文献位置调整。